Nonstoichiometry, Defect Chemistry and Oxygen Transport in Fe-Doped Layered Double Perovskite Cobaltite PrBaCo$_{2-x}$Fe$_x$O$_{6-\delta}$ (*x*=0–0.6) Membrane Materials

Ivan L. Ivanov, Petr O. Zakiryanov, Vladimir V. Sereda, Maxim O. Mazurin, Dmitry A. Malyshkin, Andrey Yu. Zuev and Dmitry S. Tsvetkov *

Institute of Natural Sciences and Mathematics, Ural Federal University, 19 Mira St., 620002 Ekaterinburg, Russia
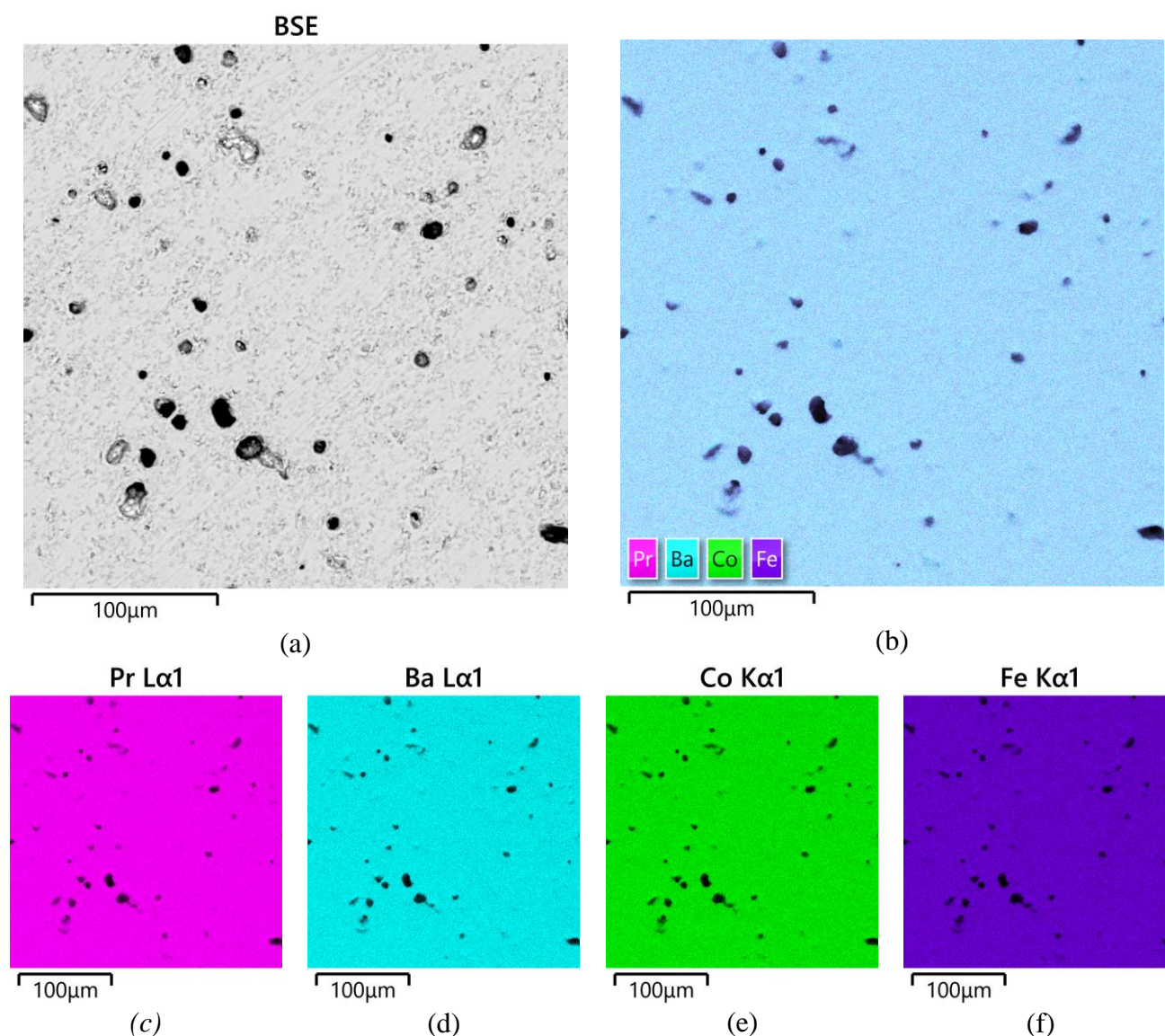
* Correspondence: dmitry.tsvetkov@urfu.ru

Figure S1. Typical results of the morphology and chemical composition study for PrBaCo$_{1.4}$Fe$_{0.6}$O$_{5.92}$, representative for all PrBaCo$_{2-x}$Fe$_x$O$_{6-\delta}$ (PBCF) samples: (**a**) electron image in the backscattered electrons (BSE) mode; element distribution maps (energy-dispersive X-ray (EDX) spectroscopy): (**b**) cumulative Pr+Ba+Co+Fe; (**c**) Pr; (**d**) Ba; (**e**) Co; (**f**) Fe.
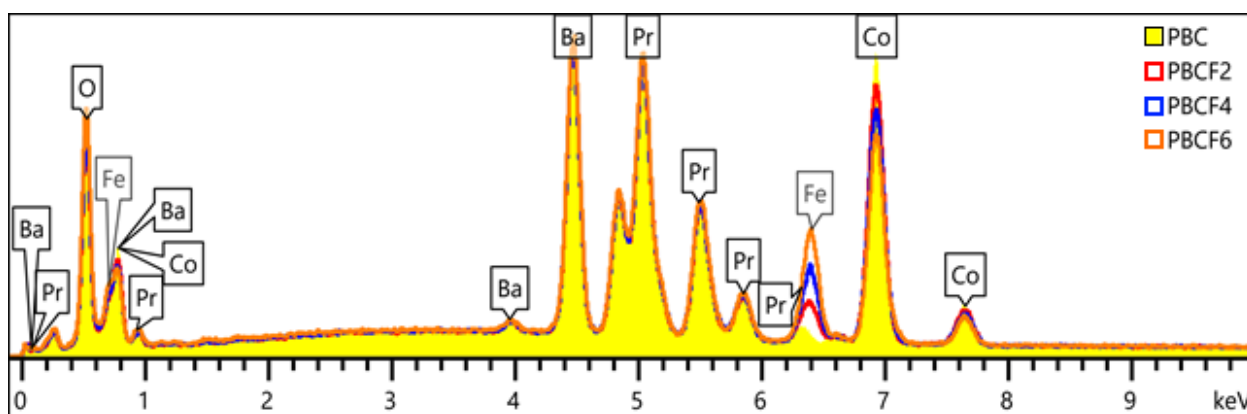
Figure S2. Typical EDX spectra of the studied samples of PrBaCo$_{2-x}$Fe$_x$O$_{6-\delta}$ (PBCF): PrBaCo$_2$O$_{5.77}$ (PBC), PrBaCo$_{1.8}$Fe$_{0.2}$O$_{5.84}$ (PBCF2), PrBaCo$_{1.6}$Fe$_{0.4}$O$_{5.87}$ (PBCF4) and PrBaCo$_{1.4}$Fe$_{0.6}$O$_{5.92}$ (PCBF6).
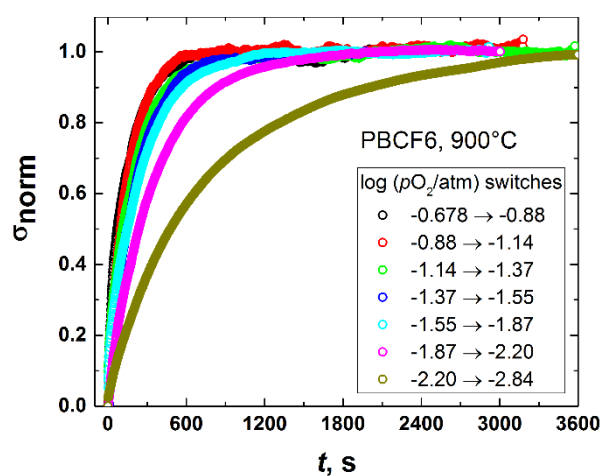

Figure S3. The normalized total conductivity of PrBaCo$_{1.4}$Fe$_{0.6}$O$_{6-\delta}$ (PBCF6) at 900 °C during the various pO$_2$ switches.
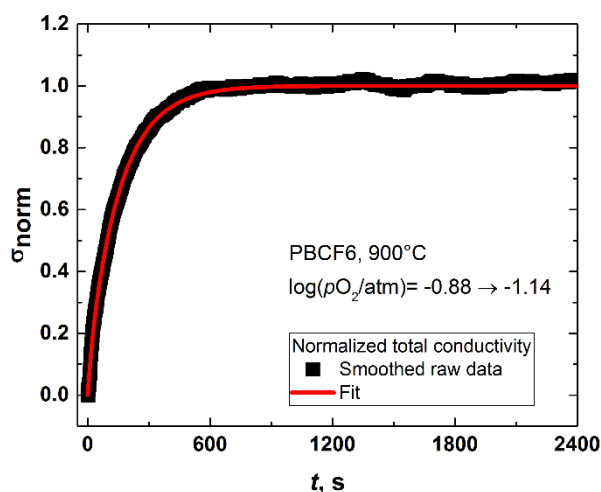

Figure S4. The result of fitting of the solution of Fick's 2nd law to the normalized total conductivity of PBCF6 at 900 °C during the log(pO$_2$/atm) switching from −0.87 to −1.13: experimental data – black squares, fitted function – red line.

Table S1. Refined lattice parameters, oxygen content and cation mass fractions in the as-prepared $PrBaCo_{2-x}Fe_xO_{6-\delta}$ (PBCF). $PrBaCo_2O_{6-\delta}$ (PBC), $PrBaCo_{1.8}Fe_{0.2}O_{6-\delta}$ (PBCF2), $PrBaCo_{1.6}Fe_{0.4}O_{6-\delta}$ (PBCF4) and $PrBaCo_{1.4}Fe_{0.6}O_{6-\delta}$ (PCBF6).

Sample	Space Group	Cell Parameters (Å)	Oxygen content	Chemical composition (wt.%)*	
				Meas.	Calc.
PBC	*P4/mmm*	$a = 3.9039 \pm 0.0001$ $b = 3.9039 \pm 0.0001$ $c = 7.6311 \pm 0.0001$	5.77 ± 0.02	Pr–28.77 Ba–28.22 Co–24.03	Pr–28.85 Ba–28.12 Co–24.13
PBCF2	*P4/mmm*	$a = 3.9029 \pm 0.0009$ $b = 3.9029 \pm 0.0009$ $c = 7.6444 \pm 0.0002$	5.84 ± 0.02	Pr-28.80 Ba–28.12 Co–21.50 Fe–2.33	Pr–28.82 Ba–28.09 Co–21.70 Fe–2.28
PBCF4	*P4/mmm*	$a = 3.9010 \pm 0.0001$ $b = 3.9010 \pm 0.0001$ $c = 7.6581 \pm 0.0003$	5.87 ± 0.02	Pr–28.79 Ba–28.12 Co–19.31 Fe–4.60	Pr–28.83 Ba–28.10 Co–19.29 Fe–4.57
PBCF6	*P4/mmm*	$a = 3.9083 \pm 0.0001$ $b = 3.9083 \pm 0.0001$ $c = 7.6776 \pm 0.0003$	5.92 ± 0.02	Pr–28.80 Ba–28.11 Co–16.82 Fe–6.80	Pr–28.82 Ba–28.09 Co–16.87 Fe–6.85

*Expanded uncertainty (95% confidence level) U =0.3 wt%.

Figure S5. In situ X-ray diffraction (XRD) patterns of PBC: (**a**) $\log(pO_2/\text{atm}) = -0.68$; (**b**) $\log(pO_2/\text{atm}) = -3$; (**c**) zoomed view of some fragments of (b) close to phase transition *P4/mmm↔Pmmm*. 1—25 °C, 2—100 °C, 3—200 °C, 4—300 °C, 5—400 °C, 6—500 C, 7—600 C, 8—700 °C, 9—800 °C, 10—900 °C, 11—1000 °C.
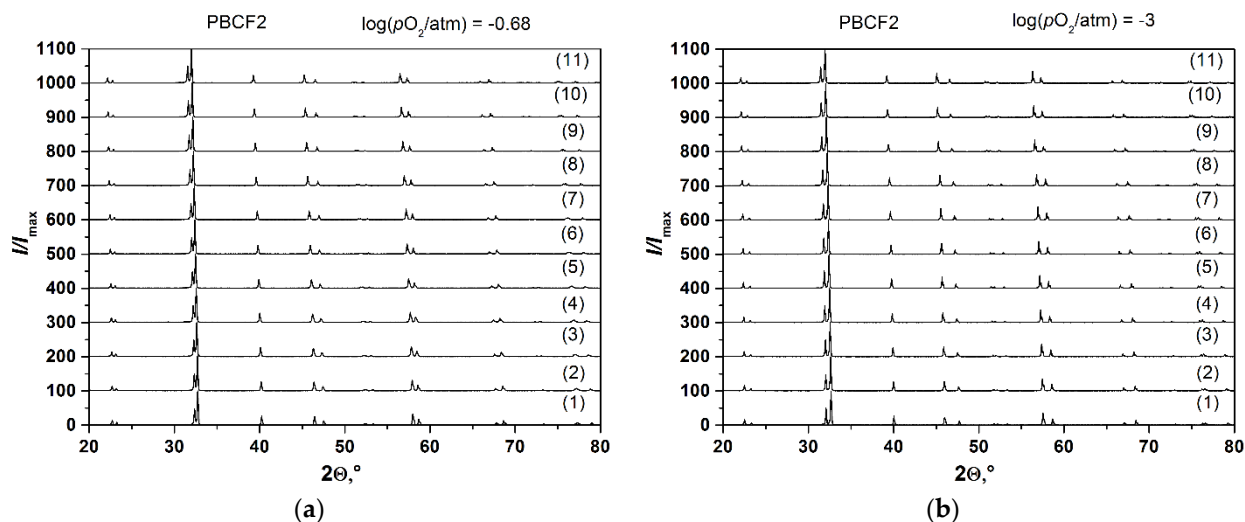
Figure S6. In situ XRD patterns of PBCF2: (**a**) log(pO₂/atm) = −0.68; (**b**) log(pO₂/atm) = −3.
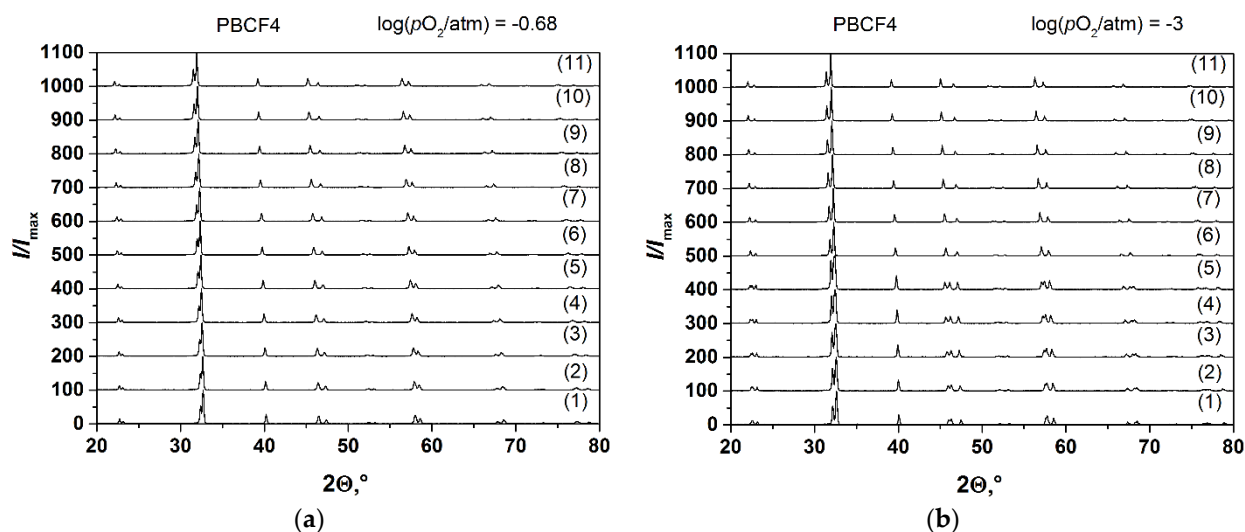1—25 °C, 2—100 °C, 3—200 °C, 4—300 °C, 5—400 °C, 6—500 °C, 7—600 °C, 8—700 °C, 9—800 °C, 10—900 °C, 11—1000 °C.
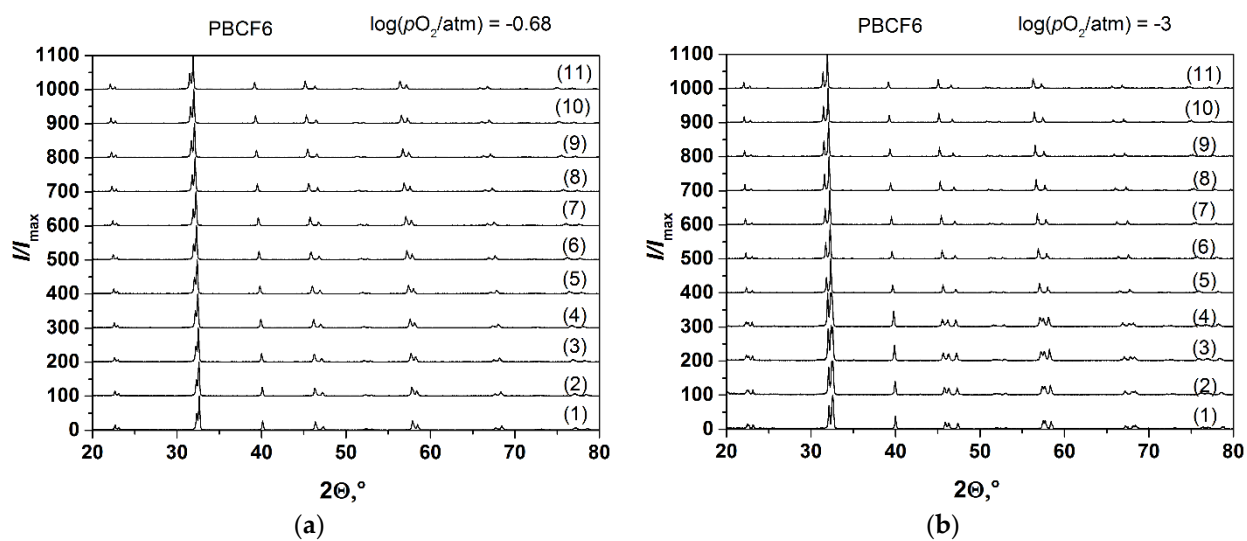

Figure S7. In situ XRD patterns of PBCF4: (**a**) log(pO₂/atm)=-0.68; (**b**) log(pO₂/atm)=-3.
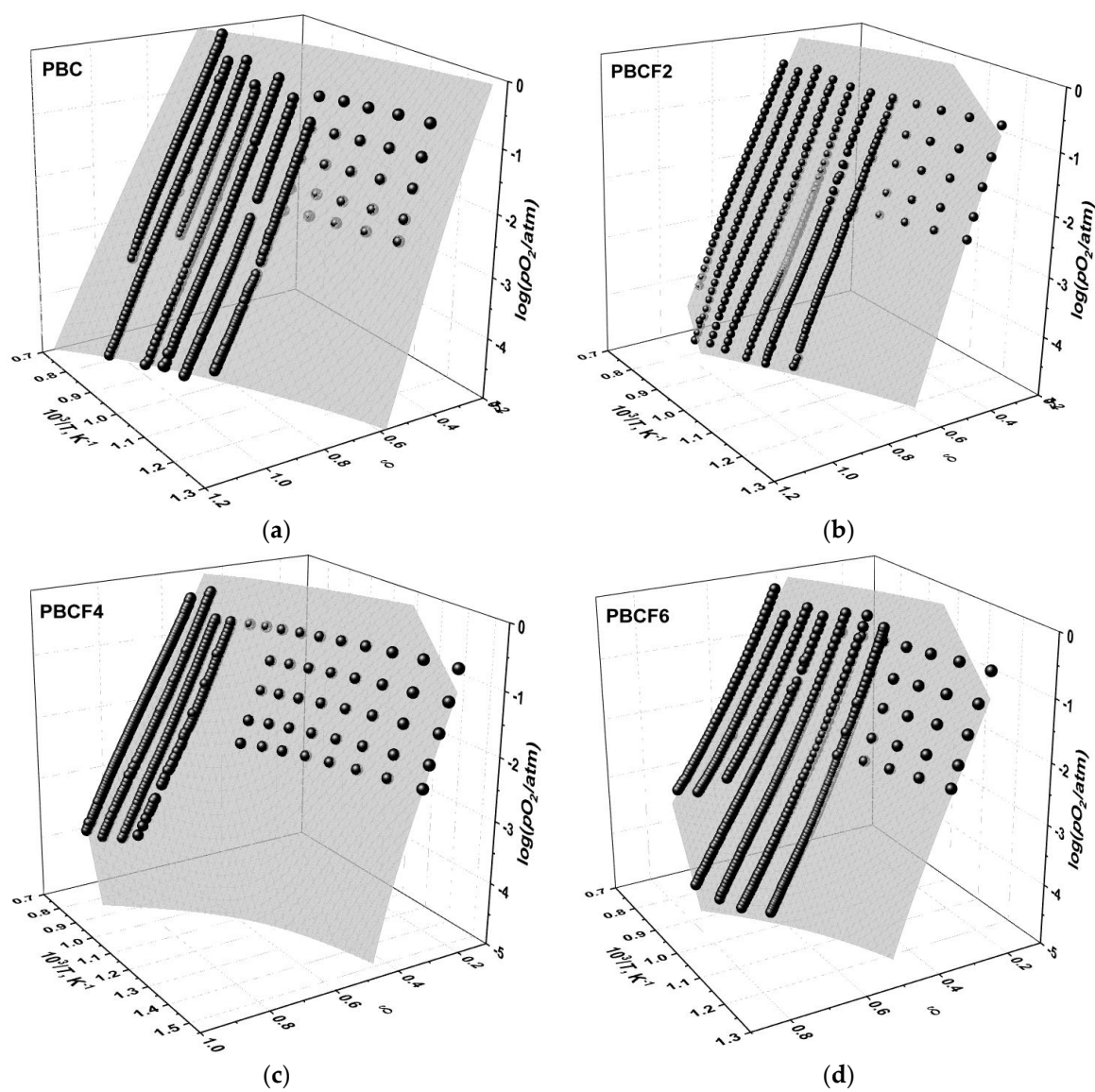1—25 °C, 2—100 °C, 3—200 °C, 4—300 °C, 5—400 °C, 6—500 °C, 7—600 °C, 8—700 °C, 9—800 °C, 10—900 °C, 11—1000 °C.

Figure S8. In situ XRD patterns of PBCF6: (**a**) log(pO$_2$/atm)=-0.68; (**b**) log(pO$_2$/atm)=-3.
1—25 °C, 2—100 °C, 3—200 °C, 4—300 °C, 5—400 °C, 6—500 °C, 7—600 °C, 8—700 °C, 9—800 °C, 10—900 °C, 11—1000 °C.

Figure S9. The results of fitting model 1 to the experimental pO_2–T–δ-datasets of (**a**) PBC; (**b**) PBCF2; (**c**) PBCF4; (**d**) PBCF6. The surfaces represent model calculations, the points—experimental data.
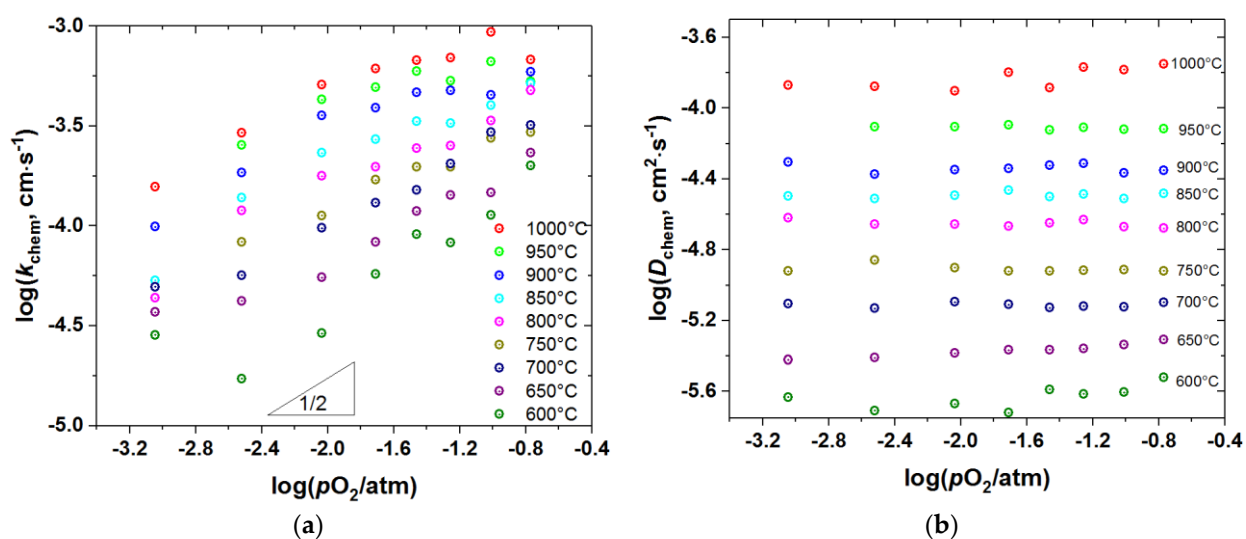
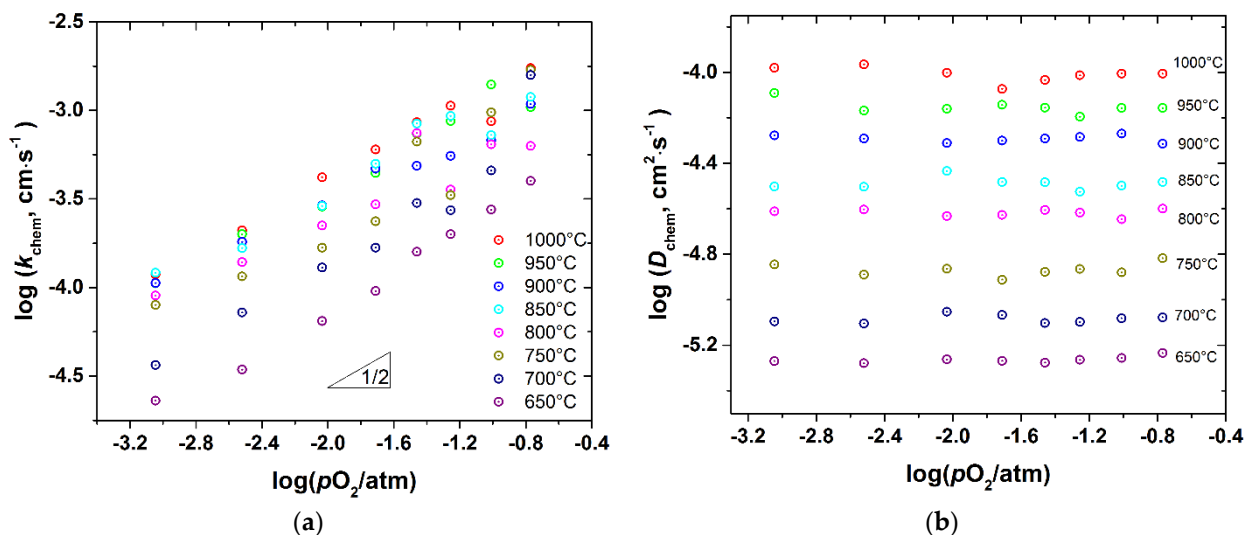**Figure S10.** The chemical surface exchange coefficient (**a**) and the chemical diffusion coefficient (**b**) of PBC vs. pO_2.

Figure S11. The chemical surface exchange coefficient (**a**) and the chemical diffusion coefficient (**b**) of PBCF2 vs. pO_2.
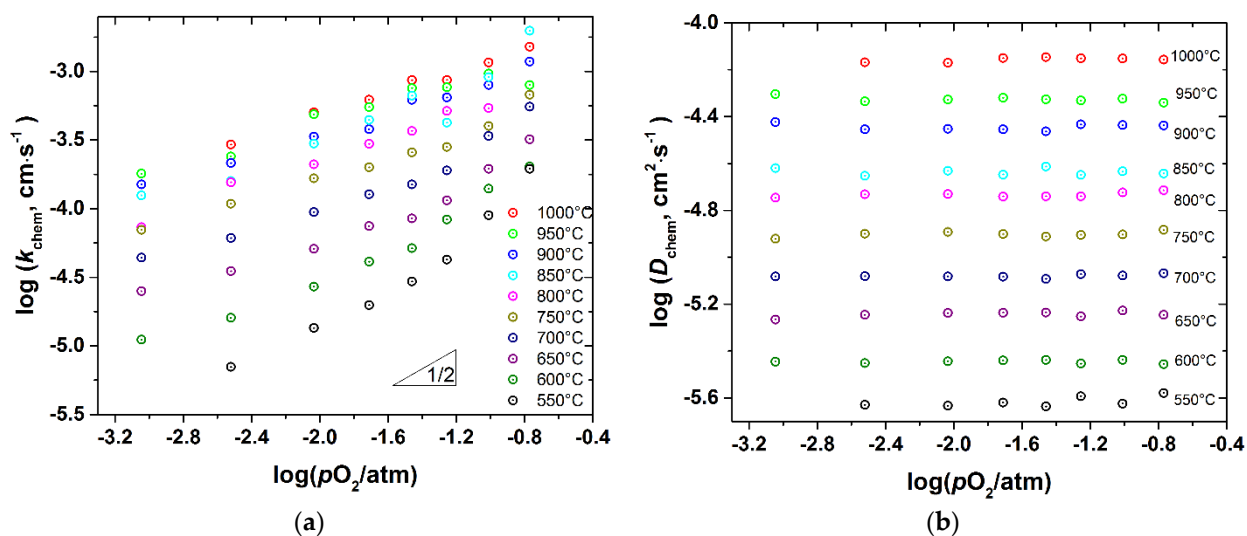
Figure S12. The chemical surface exchange coefficient (**a**) and the chemical diffusion coefficient (**b**) of PBCF4 vs. $pO2$.
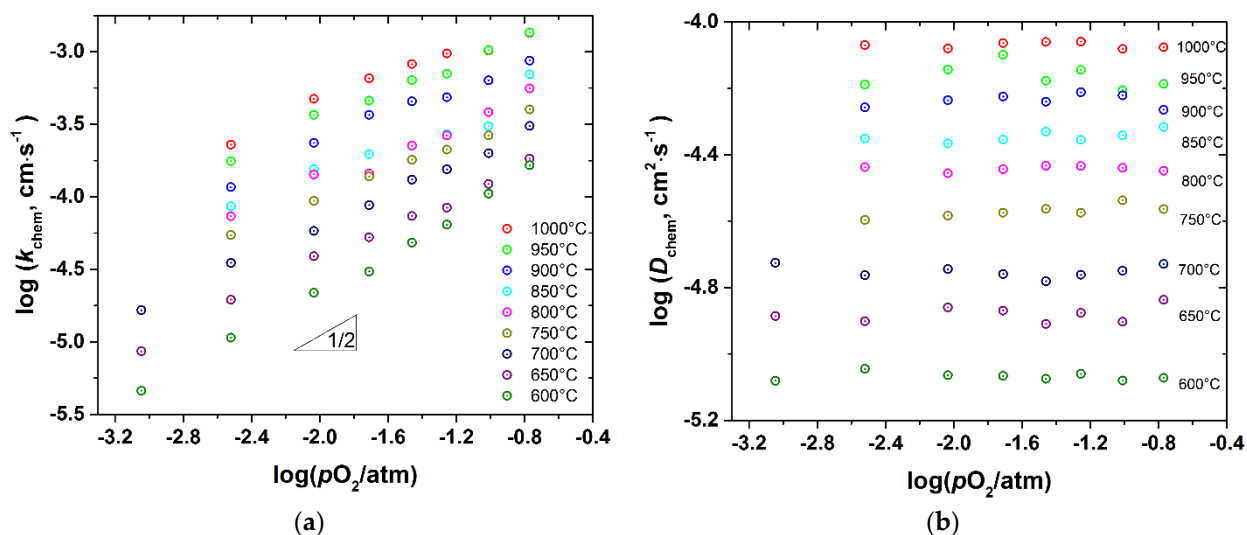

Figure S13. The chemical surface exchange coefficient (**a**) and the chemical diffusion coefficient (**b**) of PBCF6 vs. pO_2.
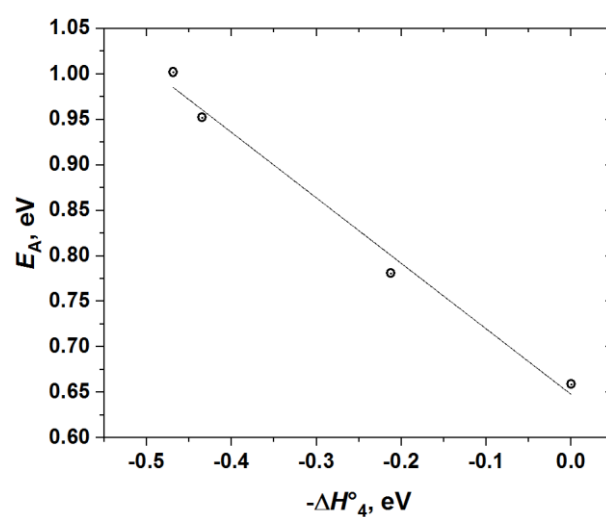
Figure S14. The activation energy of self-diffusion vs. the enthalpy of oxygen vacancies' localization in the Pr-layers for the PBCF oxides with different iron content (see also Table 2 and Figure 14 in the main text).